analytical chemistry

Article

Single-Cell Screening of Tamoxifen Abundance and Effect Using Mass Spectrometry and Raman-Spectroscopy

Ahmed Ali,[†,‡] Yasmine Abouleila,[†,‡] Yoshihiro Shimizu,[†] Eiso Hiyama,[§] Tomonobu M. Watanabe,[†] Toshio Yanagida,[†] and Arno Germond*[,†]

[†]Riken Biodynamics Research Center (BDR), 6-2-3 Furuedai, Suita, Osaka 565-0874, Japan
[‡]Research Center, Misr International University, Cairo 19648, Egypt
[§]Graduate School of Biomedical and Health Sciences, 1-2-3 Kasumi, Hiroshima, 734-0037, Japan

ⓢ *Supporting Information*

ABSTRACT: Monitoring drug uptake, its metabolism, and response on the single-cell level is invaluable for sustaining drug discovery efforts. In this study, we show the possibility of accessing the information about the aforementioned processes at the single-cell level by monitoring the anticancer drug tamoxifen using live single-cell mass spectrometry (LSC−MS) and Raman spectroscopy. First, we explored whether Raman spectroscopy could be used as a label-free and nondestructive screening technique to identify and predict the drug response at the single-cell level. Then, a subset of the screened cells was isolated and analyzed by LSC−MS to measure tamoxifen and its metabolite, 4-Hydroxytamoxifen (4-OHT) in a highly selective, sensitive, and semiquantitative manner. Our results show the Raman spectral signature changed in response to tamoxifen treatment which allowed us to identify and predict the drug response. Tamoxifen and 4-OHT abundances quantified by LSC−MS suggested some heterogeneity among single-cells. A similar phenomenon was observed in the ratio of metabolized to unmetabolized tamoxifen across single-cells. Moreover, a correlation was found between tamoxifen and its metabolite, suggesting that the drug was up taken and metabolized by the cell. Finally, we found some potential correlations between Raman spectral intensities and tamoxifen abundance, or its metabolism, suggesting a possible relationship between the two signals. This study demonstrates for the first time the potential of using Raman spectroscopy and LSC−MS to investigate pharmacokinetics at the single-cell level.
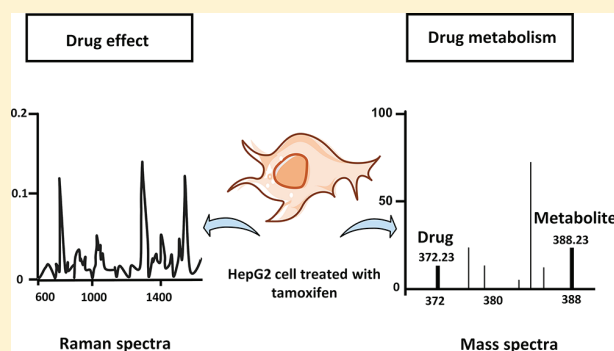
Drug discovery is a crucial aspect of medicine that has great societal impact.[1] Conventionally, the drug discovery process starts with high-throughput screening of potential chemical entities on cell populations by utilizing ensemble-averaged measurements. While convenient and informative, population-level measurements are unable to distinguish potential subpopulations[2−5] nor do they account for the heterogeneous behavior of individual cells and its effects on pharmacokinetics[6−9] and drug discovery.[10] To address this, several studies succeeded in monitoring drug interactions on the single-cell level, specifically, drug uptake[11] or cellular response.[12,13] However, these studies did not quantify the drug, at least in a semiquantitative manner, neither were they able to monitor drug-uptake, metabolism, and drug-response for the same cell. Therefore, an approach that provides semiquantitative information about these processes at the single-cell level is required.[14]

Mass spectrometry-based approaches can be used to measure drug uptake on the single-cell level. They possess the required sensitivity and selectivity while providing comprehensive information about the analyte in question in a label-free manner.[15−17] Direct sampling of the cell in its

native environment, followed by electrospray ionization (ESI) and mass spectrometry (MS) analysis is one of the approaches used for single-cell analysis.[18,19] An additional separation step such as ion mobility separation (IMS),[20,21] and capillary electrophoresis (CE)[22,23] can also be used prior to MS measurements to improve molecular coverage. Recent innovations, such as the single-probe[24,25] and the T-probe,[26] allowed for online analysis of individual cells, with the possibility of performing repeated measurements on the same cell. However, MS-based techniques are inherently destructive (with a varying degree of invasiveness), which limits the amount of information gained, especially when considering the small volume of single-cells. Arguably, the best approach to increase the information gained from single-cell measurements in a nondestructive manner is to couple noninvasive methods such as microscopic[27] or spectroscopic imaging[28,29] to MS platforms, where the multimodal data
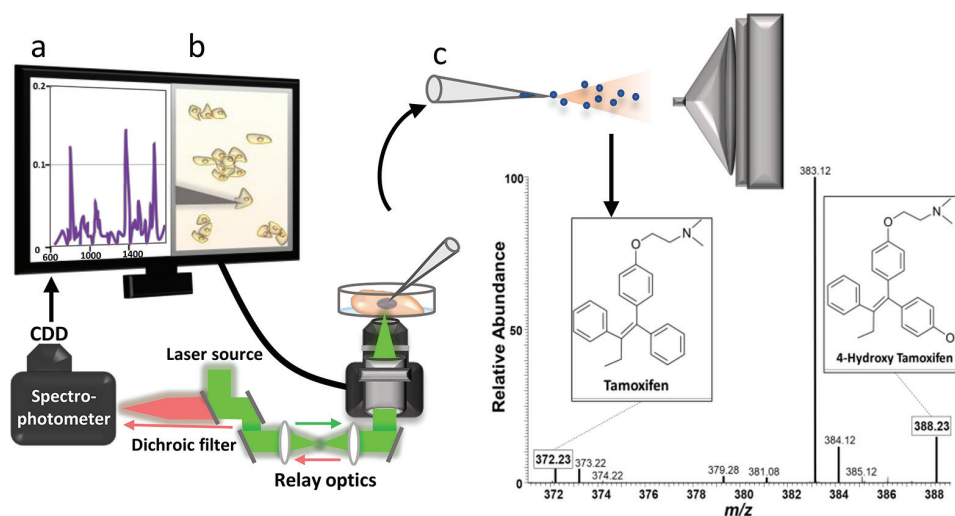
Figure 1. Schematic of single-cell analysis using Raman spectroscopy and mass spectrometry. (a) Single-cell measurement by confocal line-illumination Raman spectroscopy. A 532 nm low powered laser is focused on single living cells to acquire Raman spectra of each cell (410 cells in total). (b) After each microscopic measurement, single-cells are picked up using a tapered glass capillary attached to a micromanipulator (58 cells were sampled for MS analysis from the 410 measured by Raman spectroscopy). In 5 cells, MS measurement was not successful due to broken capillary tips, therefore, these cells were removed from subsequent data analysis. (c) The content of single-cells trapped in the capillary are analyzed by mass spectrometry after adding the ionization solvent from the opposite end of the capillary.

gained provides more information, and allows for repeated measurements of the cell (at the possible expense of throughput). However, for drug-discovery applications, higher throughput is needed to scan for cells affected by the candidate drug. To this end, it is worth exploring whether nondestructive, label-free spectroscopy can be used to perform high throughput screening of cells affected by a given drug, followed by ambient MS ionization and analysis of the same cells to monitor drug-uptake, and metabolism on the single-cell level.

Raman spectroscopy is utilized in different applications in the drug discovery process.[30−32] Notably, it has been used for studying the structure−activity relationship in molecular bindings of compounds,[33] optimizing reaction conditions and parameters,[34,35] and in pharmacokinetic studies.[36] On the single-cell level, it excels at in vivo measurement and identification of metabolic cell-states in a high throughput, nondestructive manner[37−39] which is difficult to achieve by MS. Contrarily, MS can be used in monitoring the drug and its metabolism in cells of interest in a highly selective and sensitive manner.[40] Therefore, by integrating the two approaches, one could perform untargeted monitoring of the cellular drug response using Raman spectroscopy, with the possibility of investigating the drug response of the same cells in terms of drug uptake and metabolization using mass spectrometry, all at the single cell level (Figure 1). Eventually, one could also explore the possible correlation between both signals.

In this study, we monitored the intercellular abundance of tamoxifen and its pharmacologically active metabolite (4-Hydroxytamoxifen, 4-OHT) in a selective and semiquantitative manner using live single-cell mass spectrometry (LSC−MS). Since MS is destructive, with limited throughput, we explored the use of Raman spectroscopy as a label-free screening method to identify cells that are affected by the drug. The possibility of predicting the effect of the drug on single-cells was investigated, which could be invaluable for future drug discovery applications. Furthermore, we explored the possible

correlations between relevant Raman peaks and tamoxifen or 4-OHT abundances in single-cells as measured by MS. Hepatocellular carcinoma (HepG2) cells were selected to simulate liver cells in vitro since they take-up tamoxifen, metabolize it, and are simultaneously affected by it.[41] As a proof of concept, we used two conditions (presence or absence of tamoxifen) to highlight the possibility of accessing information about the drug and its abundance by LSC−MS, as well as the drug response, as measured by Raman spectroscopy, at the single-cell level.

■ EXPERIMENTAL SECTION

Cell Culture. In this study, HepG2 cells were used to simulate liver cells in vitro. Cells were obtained from RIKEN biological resource center (BRC) cell bank. Frozen stocks stored in a liquid nitrogen tank were thawed and preheated for 1 min in 37 °C water bath (Thermo minder, Taitec Co., Saitama, Japan). Afterward, cells were grown in a culture media containing Dulbecco's Modified Eagle's medium (DMEM, Sigma-Aldrich, Minnesota, U.S.A.), supplemented with 10% fetal bovine serum (FBS) obtained from Hyclone laboratories in Utah, U.S.A. and 0.1% penicillin-streptomycin (Nacalai Tesque, Kyoto, Japan). The cells were kept for 2 days in a humidified incubator at 37 °C and 5% CO_2 (MC0−19A1C, Sanyo Electric Co., Osaka, Japan). Experiments were performed at three different days, therefore, growth phase variations had to be minimized. To do so, a pilot study was done to determine how to synchronize the growth phase of the cultured cells. Accordingly, all cultured cells were synchronized to have 50−60% confluency before drug treatment. In each experiment, cells were subcultured into 35 mm glass bottom grid dish (Matsunami, Osaka, Japan) precoated with rat-tail collagen coating solution (Cell Applications Inc., San Diego, U.S.A.), and then incubated for 24 h prior to drug treatment.

Drug Treatment. In each experiment, cells were subdivided into drug-treated and untreated subgroups, where both were washed with PBS buffer twice. Then, tamoxifen

(Sigma-Aldrich, Minnesota, U.S.A.) dissolved in dimethyl sulfoxide (DMSO, Nacalai Tesque, Kyoto, Japan) was mixed with the culture media to a final volume of 2 mL and tamoxifen concentration of 10 μM for the drug-treated group. In the untreated group, a corresponding volume of solvent (DMSO) was mixed into the medium as a control for the effect of DMSO. Both groups were further incubated for 24 h.

Raman Spectral Imaging and Spectral Preprocessing. Immediately before observation, cell cultures were taken out from the incubator, washed twice, and their medium was replaced with warmed FluoroBrite DMEM (Thermo Fisher Scientific, Massachusetts, U.S.A.). We used FluoroBrite DMEM media because it provides the same background level as PBS when measured by Raman spectroscopy, while providing better nutrition for the cells. Samples were placed into a heated microchamber (ibidi, Munich, Germany) fixed onto a motorized microscope stage (BIOS-L101T-S, Opto-Sigma, Tokyo, Japan). The microchamber was supplied with 5% CO_2 and kept at 37 °C during measurements. Raman spectral measurements were performed using a custom-built slit-scanning confocal scanning Raman microscope described in a previous study.[42] We used a line illumination system where the laser light is shaped as a plane which allow us to obtain 400 spectra in a single exposure. A 532 nm diode-pumped solid-state laser (Ventus, Laser Quantum, U.K.) was focused to a few micrometers above the optical glass surface through the objective lens (NA: 0.95, UPL40, Olympus, Tokyo, Japan). Spectra were recorded using a cooled CCD camera (PIXIS BR400, Princeton Instruments, New Jersey, U.S.A.) mounted on a polychromator. The polychromator used a 1200 g/mm grating to maximize the spectral resolution of the fingerprint region (from 600 to 1700 cm^{-1}). The spatial resolution of our system is approximately 300 nm and spectral resolution is 1 cm^{-1}.

We used glass-bottom grid culture dishes, which allowed us to perform Raman measurements on a single-cell while recording its location, then sample the cell for subsequent MS analysis. Living cells were exposed for 10 s with a laser intensity of 2.4 mW/μm^2. Single line exposure was used, and the data obtained from pixels corresponding to each single-cell were averaged. This approach minimized the time between Raman and MS measurements of the same cell. Hyper-spectral images were processed using homemade algorithms to remove cosmic-rays, perform background subtraction, baseline correction using an iterative polynomial fitting known as the ModPoly algorithm,[43] and vector-normalization, as described in our previous study.[42] In total, 410 spectra of single cells were obtained. Right after spectral measurements, single cells were picked using a custom-built capillary system for subsequent mass-spectroscopy measurements (Figure 1). To verify the reproducibility of the measurements, experiments were performed three times on different days, and in each experiment, both cells cultured in presence (approximately 80 to 120 cells) or absence of drugs (approximately 35 to 40 cells) were measured.

Multivariate Analyses of Spectral Data. To discriminate the cells treated in the absence or presence of drug, a projection on latent structure (PLS-DA) model was built using as input the spectral fingerprint region of Raman spectra (600 to 1710 cm^{-1}). The PLS is a regression model which employs the fundamental concept of principle component analysis (PCA) but further aims to maximize the covariance between the components, named Latent Variables (LVs).[44,45] PLS-DA

is a supervised machine learning technique that has been widely used on spectral data to perform a predictive analysis of known groups. To demonstrate the predictive power of the model and the generalization of our method, the normalized spectral data from two independent experiments were used as a training model, and new data from a third independent experiment was used as test data. For cross-validation of the model, a Venetian blind cross-validation with 10 splits was applied. A model with 2 components (Latent Variables) was chosen as the best model. To identify which Raman spectral peaks contributed in the discrimination of the cells, we calculated the score of Variable Importance in Projection (VIP) for each Raman wavenumbers. The VIP score of a variable is calculated as a weighted sum of the squared correlations between the PLS-DA components and the original variable.[46] It is a statistical measure of a variable's importance in the PLS-DA model which can used to select relevant predictors.[46] Analyses were performed using the eigenvector software (eigenvector Research Inc., Wenatchee, U.S.A.).

Single Cell Sampling for Mass Spectrometry Analysis. After Raman measurements of a given cell, it was immediately picked up using glass micropipettes with 3 μm bore-size. Due to the limited throughput of manual micromanipulation, only 36 treated cells and 22 untreated cells were sampled. The sampling setup included a micromanipulator attached to a platinum-coated glass capillary (CT-2, Cellomics, Hiroshima, Japan). The capillary holder was connected to a syringe to apply negative pressure on the capillary during sampling. After observing the cell of interest in the Raman microscope, the capillary holder was lowered using the micromanipulator, and the cell was sampled by applying negative pressure on the capillary with constant visual feedback from the microscope.[47] To reduce variations in the volume sampled, only cells with similar dimensions were chosen (measured by Metamorph software, Molecular devices, California, U.S.A.).

To each capillary, 2 μL of the ionization solvent were added from the wide end by using a pipet attached to eppendorf GELoader tips (Eppendorf, Hamburg, Germany). The ionization solvent used in the analysis was a mixture of 80% methanol, 10% DMSO, 0.1% formic acid. All reagents used in the ionization solvent were of LC-MS grade and were obtained from Sigma-Aldrich, Missouri, U.S.A. Furthermore, prior to measurements, 2 ng/mL (5.31 nM) of d5-tamoxifen (Cambridge Isotope Laboratories, Inc., Massachusetts, U.S.A.) was added to the ionization solvent as an internal standard. The capillary containing the ionization solvent and the cell was then attached to a nanoelectrospray adapter (nano-ESI) that is connected to the Q-Exactive mass spectrometer used in the analysis (Thermo Fisher Scientific, Massachusetts, U.S.A.).

Mass Spectrometry Measurements. MS analysis was performed using a Q-Exactive orbitrap instrument that was previously calibrated using Pierce LTQ Velos ESI calibration solution (Thermo Fisher Scientific, Massachusetts, U.S.A.). The inlet capillary temperature, spray voltage, and automatic gain control target (AGC) were adjusted to provide the highest sensitivity for tamoxifen analysis. This was done by repeated measurements of tamoxifen standard (Sigma-Aldrich, Missouri, U.S.A.) while adjusting the previously mentioned parameters one at a time. Tandem MS (MS/MS) spectra was obtained for tamoxifen and 4-OHT standards (Sigma-Aldrich, Missouri, U.S.A.) with the optimized MS method for later comparison with the sample peaks. Furthermore, an experiment was done to ensure that the media surrounding the treated cells did not

contain tamoxifen or 4-OHT after washing. The media surrounding cells treated with 10 μM tamoxifen was aspirated using a 1 μm bore-size capillary with constant visual feedback from the microscope. The volume sampled was then measured by MS, tamoxifen and 4-OHT peaks were not found in the surrounding media (Figure S-1 of the Supporting Information, SI).

During the experiments, both selective ion monitoring (SIM) and MS/MS were used to identify the analytes in question using their exact mass and fragmentation patterns. More information can be found about the instrument parameters and the MS analysis method in Table S-1. It is worth noting that some tamoxifen metabolites shared similar fragmentation patterns (mainly the fragments at m/z 58.06, m/z 72.08, and m/z 91.05) due to having closely related parent ions.[48] Therefore, while both exact mass and MS/MS were used initially for verification, relative quantitation was done by monitoring the exact mass values of the analytes in question. All detected peaks were measured with less than 3 ppm error margin in their respective m/z values.

Mass Spectrometry Data Processing and Analysis. After MS measurements, peak areas were exported from the manufacturer proprietary raw format to text files using an in-house script. Each file contained the extracted ion chromatogram (XIC) of the peaks of interest. The files were then imported into R statistical software[49] for processing and analysis. For each peak, its XIC was divided by that of the internal standard that was obtained in the same MS scan to account for the small variations between scans. The peak ratios of tamoxifen or 4-OHT and d5-tamoxifen were then log-transformed to reduce skewness. Out of the 36 tamoxifen-treated cells sampled, 5 could not be measured by MS due to broken capillary tips and were removed from subsequent analyses. Tamoxifen metabolism was calculated by dividing the abundance of metabolized tamoxifen (4-OHT) to unmetabolized tamoxifen in each cell. Correlation studies were done by calculating the Pearson correlation coefficient using a two-tailed test. All plots were done using ggplot2 package[50] in R statistical software.

Safety Considerations. During Raman operation possible eye injury could occur from the laser. Laser safety goggles should be worn to mitigate this risk.

The glass capillaries used for sampling cells have sharp tips and could cause injury with improper handling. Forceps should be used to handle the capillaries, and gloves should be worn at all times.

The ionization solvent should be prepared in a fume hood since methanol is toxic and flammable, and formic acid is corrosive and volatile.

Unlike traditional ESI interfaces, the nano-ESI is an open interface. Therefore, care should be taken to not touch the ion source during measurement to avoid possible injury.

■ RESULTS

Raman Spectroscopy Is Able to Detect and Predict the Drug Effects at Single Cell-Level. First, we explored the possibility to do a screening of the effects of drugs using nondestructive, label-free, confocal Raman microscope. We analyzed the fingerprint region ($\sim$600 to $\sim$1750 cm^{-1}) of the spectrum of living single cells. The average spectra of cells cultured in the presence or in absence of tamoxifen is shown in Figure 2a. A visual comparison of the normalized spectral intensities showed various differences in the averaged spectral
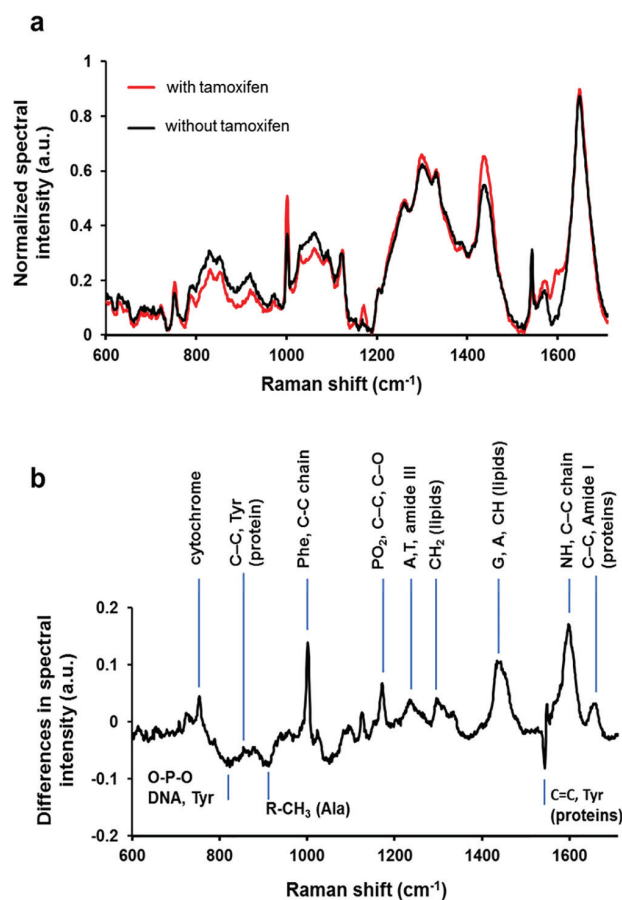
Figure 2. Spectral analysis of the fingerprint profile of single-cells measured by Raman spectroscopy. (a) Average Raman spectra of HepG2 cells cultured in presence (red line, n = 295) or absence of drug (black line, n = 115). (b) Spectral intensities of cells cultured in the presence of tamoxifen subtracted by the averaged spectrum of cells cultured in the absence of drug. Peaks for which strong differences were observed are highlighted and annotated with their associated molecular bonds or compounds identified from the literature.[42,51,52]

intensities between the two culture conditions. To highlight these differences, we calculated the differences between the spectral intensities of cells cultured in the presence of tamoxifen and the average spectrum of the cells cultured in the absence of drug (Figure 2b). Peak annotations were performed following previous studies.[42,51,52] The peak at $\sim$752 cm^{-1}, associated with cytochrome, and the peaks at $\sim$818, $\sim$851, $\sim$922, $\sim$1001, $\sim$1060, $\sim$1170, $\sim$1236, $\sim$1296, $\sim$1445, $\sim$1545, $\sim$1601, and $\sim$1651 cm^{-1} showed significant differences (ANOVA, Tukey HSD, $p < 0.05$) between cells cultured with or without tamoxifen. These differences demonstrate that the drug exposure results in a significant modification of the spectral fingerprint suggesting that the identified peaks may be considered as potential indicators of the drug effect on the metabolism of the cells, although the current experiment cannot verify the specificity of the peaks.

The reproducibility of our results was checked by performing three independent experiments on different days. Spectral differences (Figure S-2) and principal component analysis (Figure S-3) showed that difference in culture conditions (presence of absence of tamoxifen) overcome technical and

biological variations from different experiments, highlighting the reproducibility of the measurements (SI Results).

To demonstrate if the spectral signature of single-cells can discriminate between cells treated with tamoxifen and untreated cells, we used a predictive model (PLS-DA, Figure 3b). To account for technical variations, we combined the data

a

b
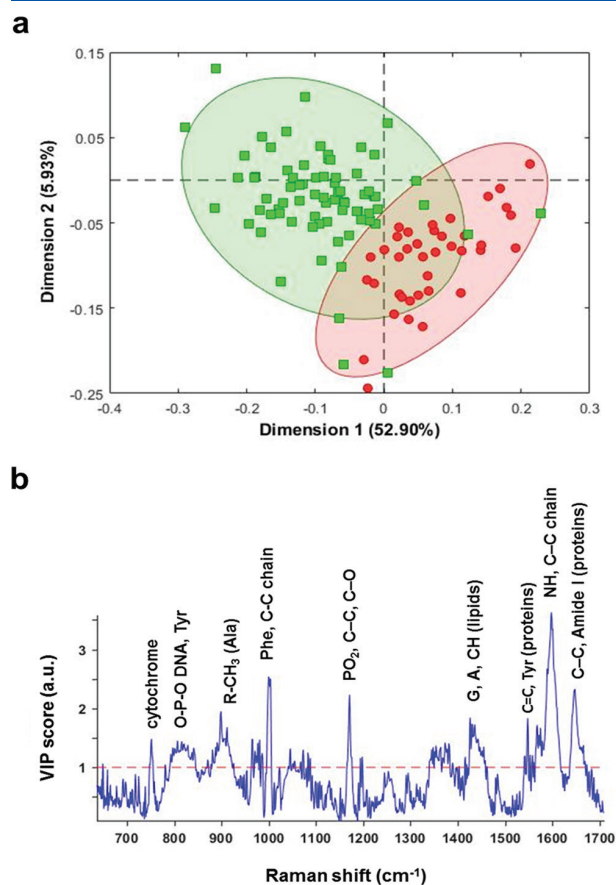
Figure 3. Predictive model of drug effect on cell metabolism and associated spectral biomarkers. (a) PLS-DA model of HepG2 cells cultured in presence (circle dots) or absence (square dots) of drug. In this analysis, only the predicted data (test data, from an independent experiment) are shown. Ellipses represent 95% confidence interval for each cluster. (b) VIP scores associated with the predictive model. The VIP scores show that the peaks contributing the most to the discrimination of the two culture conditions. Most of the peaks are similar to those observed when calculating spectral differences (Figure 2b).

across several experiments. The ability to predict the data of an independent experiment when the model is trained from the data of other independent experiments would demonstrate a good reproducibility of our experimental setup and analysis. Thus, data sets of two experiments were combined to be used as a training data set ($n = 290$), and the new spectra of cells of the third experiment were used as a test data ($n = 120$), as suggested in other studies.[42] The model aims to predict the class information (treated and untreated cells) from the spectral information used as input. Details of the test results are provided in (Table S-2). Sensitivity is the proportion of samples correctly identified as belonging to a given group, while specificity is the proportion of samples not belonging to

a given group and identified as such. Cross-validation within the training data exhibited 94.7% sensitivity when aiming to identify cells cultured with tamoxifen. When tested against the test data (Figure 3a), the predictive ability to classify the cells cultured in the presence of tamoxifen reached 100% sensitivity and 72.0% specificity (Table S-2). These results showed that our experimental approach could accurately predict the samples affected by tamoxifen, even when considering new data obtained from a separate experiment.

In an attempt to extract the spectral wavelengths (i.e., Raman shift) that contributed to the discrimination model, we calculated the VIP scores which give information about which Raman shift are the most informative to the classification (Figure 3b). The VIP scores showed that the peaks at wavenumbers ~752, ~818, ~900, ~1001, ~1170, ~1445, ~1545, ~1601, and ~1651 cm^{-1} were particularly dominant in their contribution to the classification model (Figure 3b). A strong similarity is observed with the various peaks highlighted in Figure 2b, suggesting that most of the peaks for which spectral intensities are strongly different between the two culture conditions are likely responsible for the discrimination of these conditions in the PLS-DA model.

In the above analysis, all available spectral data obtained from single-cells were used to ensure a sufficient number of samples in our model ($n = 410$). From those cells, 53 cells were sampled and analyzed by Mass spectrometry. To verify that the effects of tamoxifen can still be predicted on this smaller subset, we performed PLS-DA analysis using the spectral profiles of these cells only. Despite the smaller subset, we could successfully discriminate and predict cells that underwent tamoxifen treatment with a cross validated sensitivity of 87.5% (Figure S-4, Table S-3).

To check if tamoxifen can appear in the Raman spectra of single-cells as a results of intracellular uptake of the drug, we compared the spectral profile of tamoxifen solution, with that of cells affected by the drug. Tamoxifen peaks were not found in cells affected by the drug (Figure S-5), for more details, see the SI.

LSC−MS Can Monitor Tamoxifen and 4-OHT in Single-Cells. We evaluated the capability of LSC−MS[47] to monitor drug abundance in single cells by analyzing cells treated with tamoxifen and untreated cells previously measured by Raman spectroscopy. In total, 31 tamoxifen-treated cells and 22 untreated cells were individually analyzed by MS. Intact tamoxifen and 4-OHT [M + H]+ ions could be detected successfully at m/z 372.23 and m/z 388.23, respectively (Figure S-6). Both tamoxifen and 4-OHT were confirmed by their MS/MS fragmentation pattern (Figures S-7 and S-8). Fragmentation patterns were compared to that of previously obtained spectra of standards, and the MetFrag database for confirmation.[53]

Tamoxifen Abundance and Its Metabolism Exhibit Strong Variation Across Single-Cells. To investigate the extent of variation in tamoxifen abundance and metabolism in single-cells, the variation of tamoxifen and 4-OHT was studied across cells treated with the drug and compared with the variation in background peaks in untreated cells which represent technical variations (Figure 4a). The percent relative standard deviation (%RSD) of tamoxifen and 4-OHT in treated cells was found to be 151% and 238% RSD, respectively, while their corresponding background peaks in untreated cells exhibited 17% and 12% RSD, respectively. This disparity showed both the relatively low instrumental variations
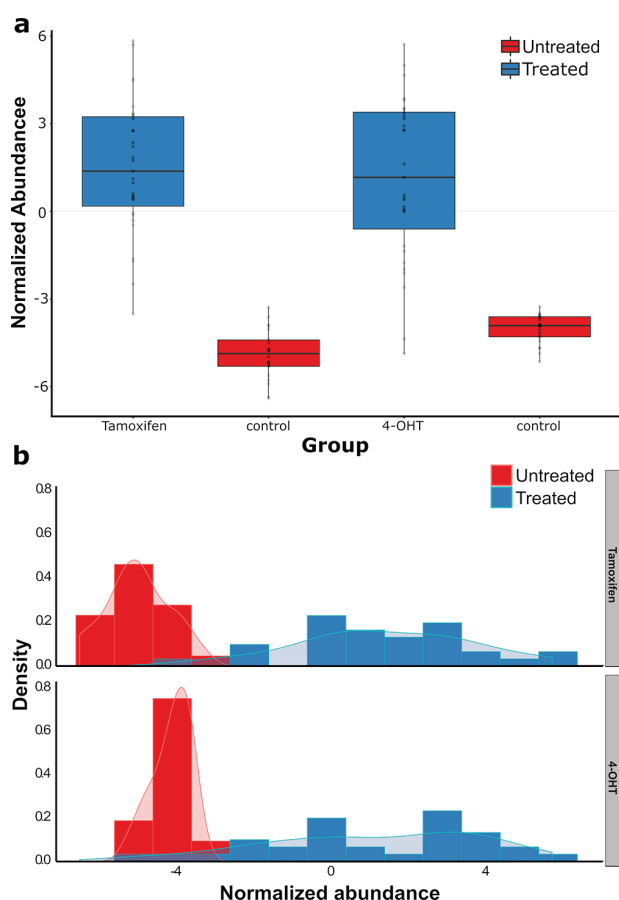
Figure 4. Distribution of tamoxifen and 4-OHT abundance in drug-treated cells and their corresponding noise peaks in untreated cells. (a) Boxplot of tamoxifen and 4-OHT normalized abundance values in tamoxifen treated cells and corresponding background peaks in untreated cells. (b) Density plot showing the broad distribution of tamoxifen and 4-OHT in tamoxifen treated cells, in contrast with corresponding background peaks in control cells that represent instrumental variation.

caused by LSC−MS and the large heterogeneity in the distributions of both tamoxifen and its metabolite in single cells.

To further study the distribution of tamoxifen and 4-OHT across single cells, a density plot of tamoxifen and 4-OHT's abundance in tamoxifen-treated cells as well as the corresponding background peaks in untreated cells was made (Figure 4b). Both tamoxifen and 4-OHT abundances show a broad distribution across single-cells, especially when contrasted against the distribution of background peaks in untreated cells. The distribution of tamoxifen metabolism across the 31 cells was studied by calculating the ratio of metabolized tamoxifen (4-OHT) and unmetabolized tamoxifen for each cell, where it exhibited 222% RSD in its distribution.

To verify that the 4-OHT signal resulted from the metabolization of tamoxifen, we studied the correlation between the drug and its metabolite (Figure S-9). Tamoxifen and 4-OHT abundances in treated cells were found to be potentially positively correlated, with a correlation coefficient of 0.54 and a p-value of 0.001 ($n = 31$).

Possible Linear Relations Were Found between Raman Data and LSC−MS Data. Raman spectral profiles represent the global signature of the drug response, while the Raman peaks shown in Figures 2b and 3b discriminated between cells affected by the drug and control cells. We explored whether those peaks could correlate with MS data and therefore would be representative of variations in tamoxifen abundance or its metabolism in a linear manner.

Few potential correlations were found. The lipid/protein/unsaturated fatty acid peak at wavelength 1651 cm^{-1} positively correlated with tamoxifen abundance ($r = 0.35$, $p = 0.045$). However, 4-OHT's abundance in single-cells correlated positively with the phenylalanine/protein peak at 1001 cm^{-1} ($r = 0.55$, $p = 0.001$), and the nucleic acid/protein/lipid peak found at 1236 cm^{-1} ($r = 0.40$, $p = 0.020$), whereas it was negatively correlated with the protein peak at 1545 cm^{-1} ($r = -0.38$, $p = 0.030$). Data are summarized in Table S-4 and Figure S-10. Moreover, we also investigated how tamoxifen metabolism (calculated by the ratio of 4-OHT to tamoxifen in each cell) could correlate with the spectral intensities of Raman peaks identified above. Tamoxifen metabolism showed two 2 possible correlations with Raman peaks 851 and 900 cm^{-1} ($p < 0.05$), with correlation coefficients of 0.35 and 0.37, respectively, and two possible negative correlations with Raman peaks at 1545 and 1651 cm^{-1} ($p < 0.05$), both having a correlation coefficient of -0.39 (Table S-4). Finally, we studied the relationship between tamoxifen metabolism and the peak ratios of the Raman peaks identified in our model. Peak ratios of 20 Raman peak pairs correlated with tamoxifen metabolism in single-cells ($p < 0.05$), with correlation coefficients ranging from -0.86 to 0.87 (Table S-5). Despite the weak correlations, these data support the existence of a few linear relations between Raman spectral data and MS data.

High and Low Tamoxifen Metabolizers Show Raman Spectral Differences. In order to investigate the possible relationship between the metabolic activity of cells and Raman spectra, tamoxifen treated cells measured by MS were divided into two groups, high and low metabolizers of tamoxifen. This was done by calculating the ratio between metabolized (4-OHT) and unmetabolized tamoxifen for each cell. Then we determined the first and fourth quartiles from the distribution of the ratios and selected the corresponding Raman spectra of cells. Cells in the first quartile exhibit poor tamoxifen metabolism due to the low metabolized to unmetabolized ratio, while cells in the fourth quartile exhibit high tamoxifen metabolism (high metabolized to unmetabolized ratio). Spectral signatures of cells of the first quartile ($n = 8$), and fourth quartile ($n = 8$) were averaged and compared to highlight the spectral peaks that strongly varies between the metabolization rate defined by MS data. Significant differences could be found (ANOVA, Tukey HSD $p < 0.05$) for the aromatic compounds peak at 1001 cm^{-1}, the lipid/protein peak at 1445 cm^{-1}, and the cytochrome peak at 752 cm^{-1} (Figure S-11). These peaks were previously identified in Figures 2 and 3, which confirm that these peaks could be considered as spectral biomarkers of the tamoxifen effect.

■ DISCUSSION

Our manuscript aimed to highlight the utility of Raman and LSC−MS in single-cell drug discovery applications. We demonstrated that Raman spectroscopy is able to accurately identify the cells that underwent drug treatment according to their spectral fingerprint. We also showed that a predictive

model could, from spectra of unknown cells, predict the cells that are affected by tamoxifen, in a label-free manner (Figure 3a). When using only cells measured by MS in our predictive model ($n = 53$), we could still discriminate between tamoxifen-treated cells ($n = 31$) and untreated cells ($n = 22$) with a high degree of sensitivity, showing the utility of our method in studies in which fewer number of cells are available, such as circulating tumor cells (Figure S-4 and Table S-3). Moreover, a number of important peaks for discriminating the two culture conditions were highlighted (Figures 2b and 3b), suggesting these variations might be linked to the presence of the drug itself inside cells or to metabolic variations generated by the drug. By doing a screening based on these possible spectral biomarkers, one could perform a fast screening of cells which could be beneficial in single-cell drug-discovery applications.

Tamoxifen is metabolized by the enzyme cytochrome P450, and interestingly we observed that the intensity of the peaks at 752 cm^{-1}, assigned to cytochrome, 1001 cm^{-1}, assigned to aromatic compounds, and protein peaks at 1651 cm^{-1} had increased normalized intensity in the spectra of cells cultured with tamoxifen. These peaks have been described as reliable indicators of the metabolism of cytochrome and glycolysis activity in living cells,[54] suggesting the observed variations could account for modification of the cytochrome or glycolytic activity in these cells. In single cells exposed to tamoxifen, we also observed an increased intensity in several major peaks associated with saturated lipids (at 1296 cm^{-1}, 1445 cm^{-1}). This suggests that the action of tamoxifen modified the lipid metabolism, which is consistent with previous literature.[54,55] However, to verify the above hypotheses further experiments are needed.

Tamoxifen's distribution has been studied on the patient level,[56] tumor level,[57] but not across single cells. In the second part of our manuscript, we demonstrated that for the first time, we can access the abundance of tamoxifen and 4-OHT in single-cells in a semiquantitative manner. The abundance of tamoxifen and 4-OHT revealed a strong variation among single-cells. Despite this, tamoxifen and 4-OHT were found to be potentially correlated, demonstrating the ability of our method to monitor the interrelation between the drug and its metabolite (Figure S-9). We hypothesize that the aforementioned heterogeneity has a biological, rather than, a technical origin. This is evident by the high %RSD of tamoxifen and 4-OHT in single-cells (151% and 238%, respectively, Figure 4a), as well as the high variation in tamoxifen metabolism across individual cells (222% RSD). This strong variation was also observed when HepG2 cells were treated with other drugs in a previous study done by our group.[58] Furthermore, comparative analysis between cells with low and high tamoxifen metabolism revealed spectral differences for peaks also found in our model (Figure 3b) which highlight the variation in tamoxifen metabolism on the single-cell level (Figure.S-11). Alternatively, the technical variation in our method was estimated in a previous study to be within (5%−25%).[47] In this study, it was calculated to be 17% and 12% for tamoxifen and 4-OHT, respectively. While we cannot pinpoint the exact hypothesized biological cause for the strong variations in tamoxifen abundance in single-cells, other work has implicated the cell membrane as a possible candidate.[59] In addition, variations in 4-OHT's abundance could be explained by variations in the uptake of its parent molecule, as well as, possible variations in its metabolism. The expression levels of CYP2D6 has been shown to be related to tamoxifen metabolism,[60] but the effect

of variations in its expression level on the single-cell level could be explored in future experiments.

In an attempt to explore the possible relationship between Raman spectral data and mass spectrometry data, we investigated the possible correlations between the two data sets. Although the Raman spectra is the contribution of many molecular compounds in cells, we hypothesized that some of those peaks might be correlated to tamoxifen or 4-OHT abundance in single-cells, as well as tamoxifen metabolism. Among those 13 peaks isolated by our model (Table S-4), 6 were possibly correlated to either tamoxifen, 4-OHT or the ratio between them ($p < 0.05$), while the ratios between 20 Raman peak pairs were correlated with tamoxifen metabolism. Those peaks are associated with fatty acid, lipids and proteins which is interesting since tamoxifen and 4-OHT are known to affect fatty acid oxidation, lipid metabolism and membrane dynamics.[61,62] Although the observed correlations are relatively weak, with nonsignificant FDR values, in our opinion, they imply a possible relation between the two data sets, and maybe of use as biomarkers for drug-effect screening in future studies.

Despite our emphasize on achieving high throughput and reproducibility, especially when it comes to Raman measurements, the throughput-mismatch between Raman and LSC−MS measurements needs to be minimized in future studies. On this regard, we are working on automating the most time-consuming and labor-intensive step in LSC−MS analysis which is cell sampling. Furthermore, it is unclear how the observed variations in spectral intensities could be affected by variations in drug concentration or time of drug exposure. This could be achieved by incrementally increasing the drug concentration or exposure time and observing the Raman spectral changes. Moreover, further investigations and comparative analysis using other drugs must be performed to assess the specificity of the measured Raman response to tamoxifen.

■ CONCLUSIONS

In light of our results, the combination of Raman spectroscopy and LSC−MS proved beneficial in identifying the response of single-cells to tamoxifen and measuring it and 4-OHT abundance in a semiquantitative manner. We envision that the development of comprehensive platforms capable of monitoring both the pharmacokinetics and pharmacodynamics in single-cells will allow single-cell measurements to complement ensemble-averaged measurements in the drug discovery process.

■ ASSOCIATED CONTENT

Ⓢ Supporting Information

The Supporting Information is available free of charge on the ACS Publications website at DOI: 10.1021/acs.analchem.8b04393.

> Raman results robustness; Tamoxifen detection by Raman spectroscopy; MS parameters; PLS-DA analysis (all cells); PLS-DA analysis (MS-measured cells) ; Raman peaks & MS correlation; Raman peak pairs ratios & MS correlation; Mass spectrum of media surrounding cells; Raman spectra of the three experiments; PCA of all cells measured by Raman; PLS-DA plot of cells measured by MS; Raman spectra of tamoxifen standard; Mass spectrum of tamoxifen and 4-OHT; Tamoxifen MS/MS spectrum; 4-OHT MS/MS spectrum; Tamoxifen and 4-OHT scatterplot; Raman peaks and MS peaks

scatterplots; and Raman spectra of high and low tamoxifen metabolizers (PDF)

■ AUTHOR INFORMATION

Corresponding Author
*Phone: +81-(0)-677-109-067. E-mail: arno.germond@gmail.com (A.G.).

ORCID ⊕
Ahmed Ali: 0000-0003-2157-4399

Author Contributions
A.A, Y.A., and A.G. wrote the manuscript. A.A., Y.A., and A.G. designed and performed the experiments. A.A and A.G. performed the statistical analyses. A.G., E.H, Y.S., and T.Y. supervised the project.

Notes
The authors declare no competing financial interest.

■ ACKNOWLEDGMENTS

■ REFERENCES

(1) Drews, J. *Science* **2000**, *287* (5460), 1960−1964.
(2) Amir, E.-A. D.; Davis, K. L.; Tadmor, M. D.; Simonds, E. F.; Levine, J. H.; Bendall, S. C.; Shenfeld, D. K.; Krishnaswamy, S.; Nolan, G. P.; Pe'er, D. *Nat. Biotechnol.* **2013**, *31* (6), 545−552.
(3) Kiss, M.; Van Gassen, S.; Movahedi, K.; Saeys, Y.; Laoui, D. *Cell. Immunol.* **2018**, *330*, 188−201.
(4) Altschuler, S. J.; Wu, L. F. *Cell* **2010**, *141* (4), 559−563.
(5) Zenobi, R. *Science* **2013**, *342* (6163), 1243259.
(6) Cohen, A. A.; Geva-Zatorsky, N.; Eden, E.; Frenkel-Morgenstern, M.; Issaeva, I.; Sigal, A.; Milo, R.; Cohen-Saidon, C.; Liron, Y.; Kam, Z.; Cohen, L.; Danon, T.; Perzov, N.; Alon, U. *Science* **2008**, *322* (5907), 1511−1516.
(7) Gascoigne, K. E.; Taylor, S. S. *Cancer Cell* **2008**, *14* (2), 111−122.
(8) Shen, F.; Chu, S.; Bence, A. K.; Bailey, B.; Xue, X.; Erickson, P. A.; Montrose, M. H.; Beck, W. T.; Erickson, L. C. *J. Pharmacol. Exp. Ther.* **2007**, *324* (1), 95−102.
(9) Deng, B.; Wang, Z.; Song, J.; Xiao, Y.; Chen, D.; Huang, J. *Anal. Bioanal. Chem.* **2011**, *401* (7), 2143−2152.
(10) Heath, J. R.; Ribas, A.; Mischel, P. S. *Nat. Rev. Drug Discovery* **2016**, *15* (3), 204−216.
(11) Passarelli, M. K.; Newman, C. F.; Marshall, P. S.; West, A.; Gilmore, I. S.; Bunch, J.; Alexander, M. R.; Dollery, C. T. *Anal. Chem.* **2015**, *87* (13), 6696−6702.
(12) Passarelli, M. K.; Pirkl, A.; Moellers, R.; Grinfeld, D.; Kollmer, F.; Havelund, R.; Newman, C. F.; Marshall, P. S.; Arlinghaus, H.; Alexander, M. R.; West, A.; Horning, S.; Niehuis, E.; Makarov, A.; Dollery, C. T.; Gilmore, I. S. *Nat. Methods* **2017**, *14* (12), 1175−1183.
(13) Thurber, G. M.; Yang, K. S.; Reiner, T.; Kohler, R. H.; Sorger, P.; Mitchison, T.; Weissleder, R. *Nat. Commun.* **2013**, *4*, 1504.
(14) Bunnage, M. E.; Chekler, E. L. P.; Jones, L. H. *Nat. Chem. Biol.* **2013**, *9* (4), 195−199.
(15) Comi, T. J.; Do, T. D.; Rubakhin, S. S.; Sweedler, J. V. *J. Am. Chem. Soc.* **2017**, *139* (11), 3920−3929.
(16) Spitzer, M. H.; Nolan, G. P. *Cell* **2016**, *165* (4), 780−791.
(17) Aichler, M.; Walch, A. *Lab. Invest.* **2015**, *95* (4), 422−431.
(18) Zhang, L.; Vertes, A. *Angew. Chem., Int. Ed.* **2018**, *57* (17), 4466−4477.
(19) Abouleila, Y.; Onidani, K.; Ali, A.; Shoji, H.; Kawai, T.; Lim, C. T.; Kumar, V.; Okaya, S.; Kato, K.; Hiyama, E.; Yanagida, T.; Masujima, T.; Shimizu, Y.; Honda, K. *Cancer Sci.* **2018**, DOI: 10.1111/cas.13915.
(20) Zhang, L.; Foreman, D. P.; Grant, P. A.; Shrestha, B.; Moody, S. A.; Villiers, F.; Kwak, J. M.; Vertes, A. *Analyst* **2014**, *139* (20), 5079−5085.
(21) Zhang, L.; Vertes, A. *Anal. Chem.* **2015**, *87* (20), 10397−10405.
(22) Onjiko, R. M.; Morris, S. E.; Moody, S. A.; Nemes, P. *Analyst* **2016**, *141* (12), 3648−3656.
(23) Onjiko, R. M.; Moody, S. A.; Nemes, P. *Proc. Natl. Acad. Sci. U. S. A.* **2015**, *112* (21), 6545−6550.
(24) Pan, N.; Rao, W.; Kothapalli, N. R.; Liu, R.; Burgett, A. W. G.; Yang, Z. *Anal. Chem.* **2014**, *86* (19), 9376−9380.
(25) Rao, W.; Pan, N.; Yang, Z. Applications of the Single-Probe: Mass Spectrometry Imaging and Single Cell Analysis under Ambient Conditions. *J. Visualized Exp.* **2016**, *112* DOI: 10.3791/53911
(26) Liu, R.; Pan, N.; Zhu, Y.; Yang, Z. *Anal. Chem.* **2018**, *90* (18), 11078−11085.
(27) Do, T. D.; Ellis, J. F.; Neumann, E. K.; Comi, T. J.; Tillmaand, E. G.; Lenhart, A. E.; Rubakhin, S. S.; Sweedler, J. V. *ChemPhysChem* **2018**, *19* (10), 1180−1191.
(28) Neumann, E. K.; Comi, T. J.; Spegazzini, N.; Mitchell, J. W.; Rubakhin, S. S.; Gillette, M. U.; Bhargava, R.; Sweedler, J. V. *Anal. Chem.* **2018**, *90* (19), 11572−11580.
(29) Lanni, E. J.; Masyuko, R. N.; Driscoll, C. M.; Dunham, S. J. B.; Shrout, J. D.; Bohn, P. W.; Sweedler, J. V. *Anal. Chem.* **2014**, *86* (21), 10885−10891.
(30) Gala, U.; Chauhan, H. *Expert Opin. Drug Discovery* **2015**, *10* (2), 187−206.
(31) Tipping, W. J.; Lee, M.; Serrels, A.; Brunton, V. G.; Hulme, A. N. *Chem. Soc. Rev.* **2016**, *45* (8), 2075−2089.
(32) Paudel, A.; Raijada, D.; Rantanen, J. *Adv. Drug Delivery Rev.* **2015**, *89*, 3−20.
(33) Pivonka, D. *Appl. Spectrosc.* **2004**, *58* (3), 323−331.
(34) Heinz, A.; Strachan, C. J.; Gordon, K. C.; Rades, T. *J. Pharm. Pharmacol.* **2009**, *61* (8), 971−988.
(35) Xie, Y.; Cao, W.; Krishnan, S.; Lin, H.; Cauchon, N. *Pharm. Res.* **2008**, *25* (10), 2292−2301.
(36) Farquharson, S.; Shende, C.; Inscore, F. E.; Maksymiuk, P.; Gift, A. *J. Raman Spectrosc.* **2005**, *36* (3), 208−212.
(37) Yue, S.; Cheng, J.-X. *Curr. Opin. Chem. Biol.* **2016**, *33*, 46−57.
(38) Kann, B.; Offerhaus, H. L.; Windbergs, M.; Otto, C. *Adv. Drug Delivery Rev.* **2015**, *89*, 71−90.
(39) Li, M.; Xu, J.; Romero-Gonzalez, M.; Banwart, S. A.; Huang, W. E. *Curr. Opin. Biotechnol.* **2012**, *23* (1), 56−63.
(40) Binkhorst, L.; Mathijssen, R. H. J.; Ghobadi Moghaddam-Helmantel, I. M.; de Bruijn, P.; van Gelder, T.; Wiemer, E. A. C.; Loos, W. J. *J. Pharm. Biomed. Anal.* **2011**, *56* (5), 1016−1023.
(41) Tabassum, H.; Rehman, H.; Banerjee, B. D.; Raisuddin, S.; Parvez, S. *Clin. Chim. Acta* **2006**, *370* (1−2), 129−136.
(42) Germond, A.; Ichimura, T.; Horinouchi, T.; Fujita, H.; Furusawa, C.; Watanabe, T. M. *Communications Biology* **2018**, *1* (1), 85.
(43) Lieber, C. A.; Mahadevan-Jansen, A. *Appl. Spectrosc.* **2003**, *57* (11), 1363−1367.
(44) Wold, S.; Sjöström, M.; Eriksson, L. Partial Least Squares Projections to Latent Structures (PLS) in Chemistry. In *Encyclopedia of Computational Chemistry*; Ragué Schleyer, P., Allinger, N. L., Clark, T., Gasteiger, J., Kollman, P. A., Schaefer, H. F., Schreiner, P. R., Eds; John Wiley & Sons, 2002.
(45) Eriksson, L.; Andersson, P. L.; Johansson, E.; Tysklind, M. *Mol. Diversity* **2006**, *10* (2), 169−186.
(46) Chong, I.-G.; Jun, C.-H. *Chemom. Intell. Lab. Syst.* **2005**, *78* (1−2), 103−112.

(47) Fujii, T.; Matsuda, S.; Tejedor, M. L.; Esaki, T.; Sakane, I.; Mizuno, H.; Tsuyama, N.; Masujima, T. *Nat. Protoc.* **2015**, *10* (9), 1445−1456.

(48) Heath, D. D.; Flatt, S. W.; Wu, A. H. B.; Pruitt, M. A.; Rock, C. L. *Br. J. Biomed. Sci.* **2014**, *71* (1), 33−39.

(49) R Core Team. *R: A Language and Environment for Statistical Computing*; R Foundation for Statistical Computing, Vienna, Austria, 2018, URL https://www.R-project.org/.

(50) Wickham, H. *ggplot2: Elegant Graphics for Data Analysis*; Springer, 2016.

(51) Collado, J. A.; Ramírez, F. J. *J. Raman Spectrosc.* **1999**, *30* (5), 391−397.

(52) Sasic, S. *Pharmaceutical Applications of Raman Spectroscopy*; John Wiley & Sons, 2008.

(53) Ruttkies, C.; Schymanski, E. L.; Wolf, S.; Hollender, J.; Neumann, S. *J. Cheminf.* **2016**, *8*, 3.

(54) Okada, M.; Smith, N. I.; Palonpon, A. F.; Endo, H.; Kawata, S.; Sodeoka, M.; Fujita, K. *Proc. Natl. Acad. Sci. U. S. A.* **2012**, *109* (1), 28−32.

(55) Fong, C. J.; Burgoon, L. D.; Williams, K. J.; Forgacs, A. L.; Zacharewski, T. R. *BMC Genomics* **2007**, *8*, 151.

(56) Schroth, W.; Goetz, M. P.; Hamann, U.; Fasching, P. A.; Schmidt, M.; Winter, S.; Fritz, P.; Simon, W.; Suman, V. J.; Ames, M. M.; Safgren, S. L.; Kuffel, M. J.; Ulmer, H. U.; Boländer, J.; Strick, R.; Beckmann, M. W.; Koelbl, H.; Weinshilboum, R. M.; Ingle, J. N.; Eichelbaum, M.; Schwab, M.; Brauch, H. *JAMA* **2009**, *302* (13), 1429−1436.

(57) Végvári, Á.; Shavkunov, A. S.; Fehniger, T. E.; Grabau, D.; Niméus, E.; Marko-Varga, G. *Clin. Transl. Med.* **2016**, *5* (1), 10.

(58) Fukano, Y.; Tsuyama, N.; Mizuno, H.; Date, S.; Takano, M.; Masujima, T. *Nanomedicine* **2012**, *7* (9), 1365−1374.

(59) Deng, B.; Wang, Z.-M.; Zhou, Z.-H.; Liu, Y.-M.; Yang, X.-L.; Song, J.; Xiao, Y.-X. *Biomed. Chromatogr.* **2014**, *28* (10), 1393−1401.

(60) Etienne, M. C.; Milano, G.; Fischel, J. L.; Frenay, M.; François, E.; Formento, J. L.; Gioanni, J.; Namer, M. *Br. J. Cancer* **1989**, *60* (1), 30−35.

(61) Ribeiro, M. P. C.; Santos, A. E.; Custódio, J. B. A. *Toxicology* **2014**, *323*, 10−18.

(62) Custódio, J. B.; Almeida, L. M.; Madeira, V. M. *Biochim. Biophys. Acta, Biomembr.* **1993**, *1153* (2), 308−314.

Supporting Information

Single-cell screening of tamoxifen abundance and effect using mass spectrometry and Raman-spectroscopy

Ahmed Ali [1], Yasmine Abouleila[1], Yoshihiro Shimizu[1], Eiso Hiyama[2], Tomonobu M. Watanabe[1], Toshio Yanagida[1], Arno Germond[1]*

1- Riken Biodynamics Research Center (BDR), 6-2-3 Furuedai, Suita, Osaka 565-0874, Japan
2- Graduate school of biomedical and health sciences, 1-2-3 Kasumi, Hiroshima, 734-0037, Japan.
 * *Corresponding authors:*
Arno Germond, Ph.D.
Laboratory for Comprehensive Bioimaging,
RIKEN Biodynamics Research Center (BDR),
6-2-3 Furuedai, Suita, Osaka 565-0874, Japan
Email: arno.germond@gmail.com

Table of contents:

Supplementary Results:
Reproducibility of Raman spectral measurements
Spectral measurements were performed across three independent experiments on different days. Small variations in the peak intensities were observed in the average spectra across the experiments (Fig. S-2). However, a comparison of spectral intensities clearly shows that the differences in culture condition (presence or absence of tamoxifen) are more important (Fig. S-2). For example, the normalized intensity of the peak at ~1601 cm^{-1} was consistently higher for cells cultured in presence tamoxifen than without (ANOVA, Tukey HSD, $p < 0.05$)(Fig. S-2). To study the variations across experiments and compare it to variations across the two culture conditions, we use Principal Component Analysis (PCA). When plotting the average spectrum of individual cells in a PCA space, some cluster seemed to emerge in the first two dimensions, suggesting the differences between the presence or absence of drug could allow discrimination of cells (Fig. S-3a). On the other hand, when coloring cells differently depending on their experiment in the same PCA space (Fig. S-3b), we noticed no particular cluster between the three independent experiments, suggesting the differences observed across experiments are not dominant.

Cellular tamoxifen cannot be directly detected by Raman spectroscopy
For a comparative purpose, we measured the spectrum profile of a solution of tamoxifen, which revealed its major peaks (Fig. S-5). However, when measuring cells affected by tamoxifen, the major peaks of tamoxifen were not found in the spectra of living cells. In our opinion, it is unlikely that tamoxifen could appear in the Raman spectra of single cells as a result of the intracellular uptake of the drug, because for the concentrations used in cell culture, the drug or its metabolite are expected in nM concentration in single cells, which is far below the sensitivity of a spontaneous Raman confocal system. Therefore, we hypothesize that the variations monitored in several Raman peaks resulted from a complex metabolic response (including the influence of protein, lipids, etc.) of HepG2 cells following the drug exposure.

Table S-1. SIM mode and tandem-MS scan parameters. All parameters were optimized by repeated measurement of tamoxifen standard targeting the best sensitivity.

Instrumental variable	Value
Spray voltage	1500 v
Capillary temperature	400℃
S-lens RF level	90%
SIM range	347-397 m/z
SIM AGC target	5.00E+06
SIM maximum injection time	200 ms
SIM resolution	140,000 FWHM
MS/MS range	50-400 m/z
MS/MS AGC target	2.00E+05
MS/MS maximum injection time	100 ms
MS/MS resolution	17,500 FWHM
MS/MS isolation window	1 m/z
MS/MS Normalized collision energy (NCE)	35

Table S-2. Detailed results of the PLS-DA analysis (n = 410). Data from two independent experiments were combined to predict the presence or absence of tamoxifen effects on cells measured in a third independent experiment. Abbreviations are Calibrated (Cal), Cross-Validation (CV) and Predicted (Pred).

Model parameters	Cells cultured in presence of tamoxifen	Cells cultured in absence of tamoxifen
Sensitivity (Cal)	0.977	1.000
Specificity (Cal)	1.000	0.977
Sensitivity (CV)	0.964	0.947
Specificity (CV)	0.947	0.964
Sensitivity (Pred)	0.720	1.000
Specificity (Pred)	1.000	0.720
RMSE (Cal)	0.34342	0.777447
RMSE (CV)	0.37909	0.794571
RMSE (Pred)	0.356542	0.954356

Table S-3. Detailed results of the PLS-DA analysis of samples analyzed by mass spectrometry after Raman measurements (n = 53). PLS-DA analysis was performed on cells that were measure by mass spectrometry only (n = 31 treated cells, n = 22 untreated cells). Test data were randomly chosen to account for 22% of the dataset (tamoxifen, n = 7, control n = 5). Abbreviations are Calibrated (Cal), Cross-Validation (CV) and Predicted (Pred).

Model parameters	Cells cultured in presence of tamoxifen	Cells cultured in absence of tamoxifen
Sensitivity (Cal)	1.000	0.706
Specificity (Cal)	0.706	1.000
Sensitivity (CV)	0.875	0.706
Specificity (CV)	0.706	0.875
Sensitivity (Pred)	0.857	0.600
Specificity (Pred)	0.600	0.857

Table S-4. Correlations values for 13 peaks that were identified in Figure 2b and 3b with MS data. We explored the possibility for linear relations with the abundance of tamoxifen or its metabolite or the metabolic activity (4-OHT : tamoxifen ratio) as measured by mass-spectrometry in the 31 treated cells.

Raman peak	Correlation coefficient (tamoxifen)	p-value (tamoxifen)	Correlation coefficient (4-OHT)	p-value (4-OHT)	Correlation coefficient (Tamoxifen metabolism)	P-value (Tamoxifen metabolism)
752 cm^{-1}	0.03	0.884	-0.13	0.459	0.04	0.824
818 cm^{-1}	-0.18	0.301	-0.06	0.733	0.25	0.146
851 cm^{-1}	-0.19	0.278	0.02	0.898	0.35	0.044
900 cm^{-1}	-0.21	0.226	0.18	0.312	0.37	0.033
1001 cm^{-1}	-0.33	0.060	0.55	0.001	0.10	0.566
1060 cm^{-1}	-0.27	0.129	-0.21	0.217	-0.04	0.815
1170 cm^{-1}	-0.06	0.744	-0.11	0.537	0.09	0.613
1236 cm^{-1}	0.18	0.310	0.4	0.020	-0.18	0.315
1296 cm^{-1}	0.03	0.846	-0.07	0.675	-0.05	0.796
1445 cm^{-1}	0.07	0.715	0.03	0.854	-0.16	0.517
1545 cm^{-1}	-0.04	0.822	-0.38	0.030	-0.39	0.022
1601 cm^{-1}	0.03	0.850	-0.13	0.479	-0.14	0.418
1651 cm^{-1}	0.35	0.045	-0.08	0.653	-0.39	0.020

Table S-5. Correlations between Raman peak pairs ratios identified in Figure 2b and 3b and tamoxifen metabolism**.** We explored the possibility for linear correlations between the 4-OHT : Tamoxifen ratio (Tamoxifen metabolism) measured by mass spectrometry and ratios of peaks identified in Fig 2b and 3b. 31 cells where used for the correlation studies. 20 ratios of Raman peak pairs where found to be correlating with Tamoxifen metabolism in cells.

Raman peak ratio	Correlation coefficient	p-value
1170/1001	-0.86	< 0.001
1060/1001	-0.86	< 0.001
1296/1001	-0.86	< 0.001
922/851	-0.84	< 0.001
1601/1001	-0.83	< 0.001
1060/851	-0.82	< 0.001
1170/851	-0.8	< 0.001
1445/1001	-0.65	< 0.001
1545/1001	-0.64	< 0.001
1236/1001	-0.64	< 0.001
1296/851	-0.53	0.001
1545/851	-0.47	0.005
1651/1445	-0.46	0.006
1651/1545	-0.43	0.011
1651/1601	-0.42	0.012
1601/851	-0.36	0.035
1545/1445	0.45	0.008
1545/1236	0.56	0.001
1651/851	0.76	< 0.001
1651/1001	0.87	< 0.001
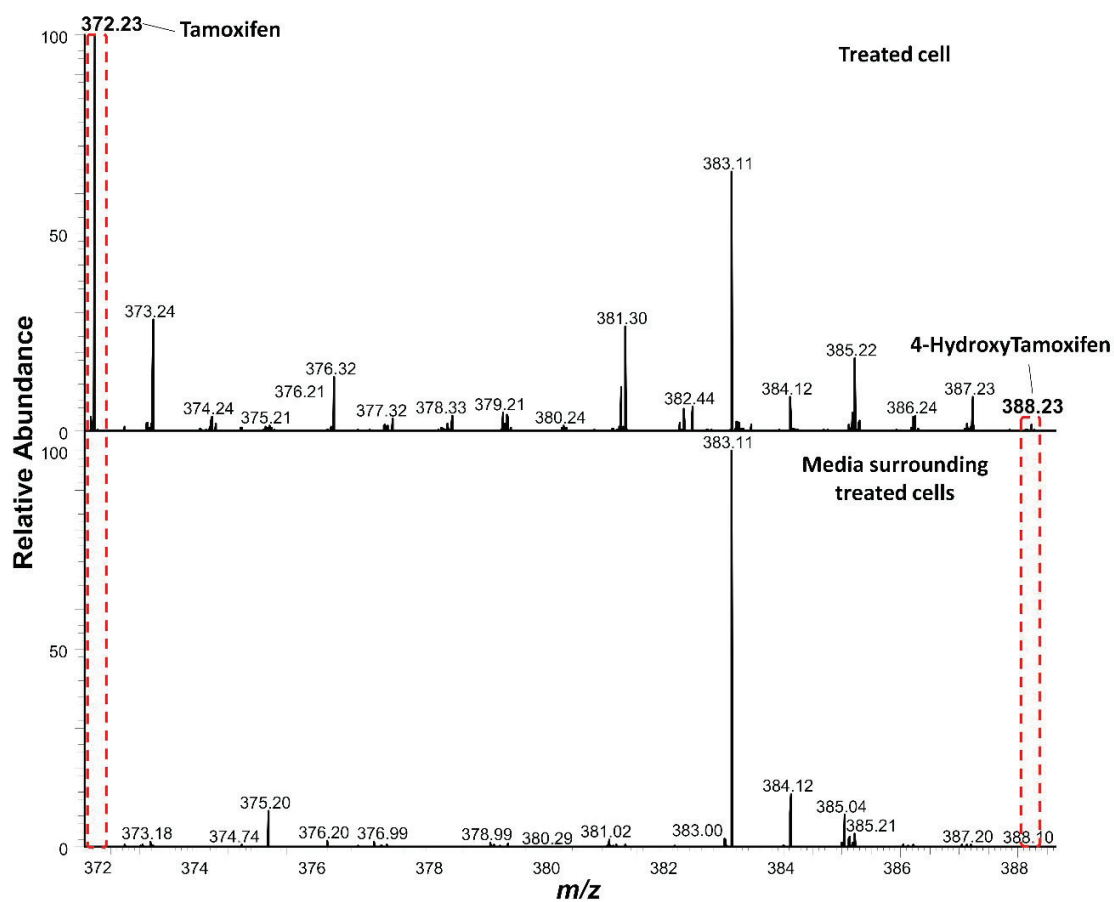
Figure S-1. Mass spectra of tamoxifen treated single cell compared with its surrounding media. Tamoxifen and 4-OHT peaks can be observed in cells treated with tamoxifen, while they cannot be observed in the surrounding media of the same cells.
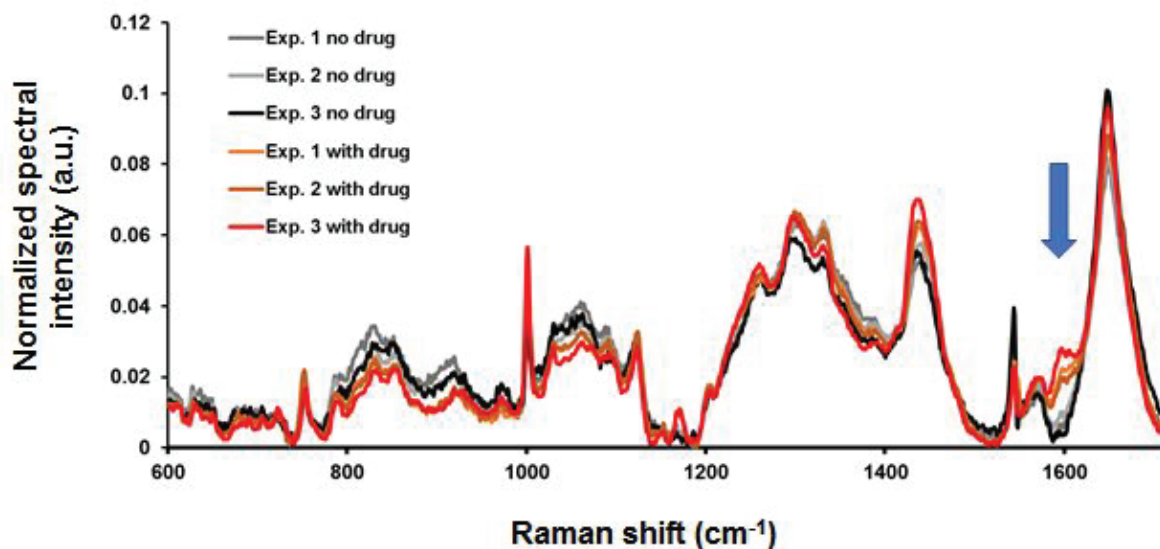
Figure S-2. Average spectrum of three independent experiments of single cells cultured in the presence ("with drug") or absence of tamoxifen ("no drug"). Differences are observed between the two culture conditions were consistent for several peaks across the spectral range. The indicated arrow highlights one example peak for which differences between the conditions are the most extreme, and in a reproducible manner across the three independent experiments.
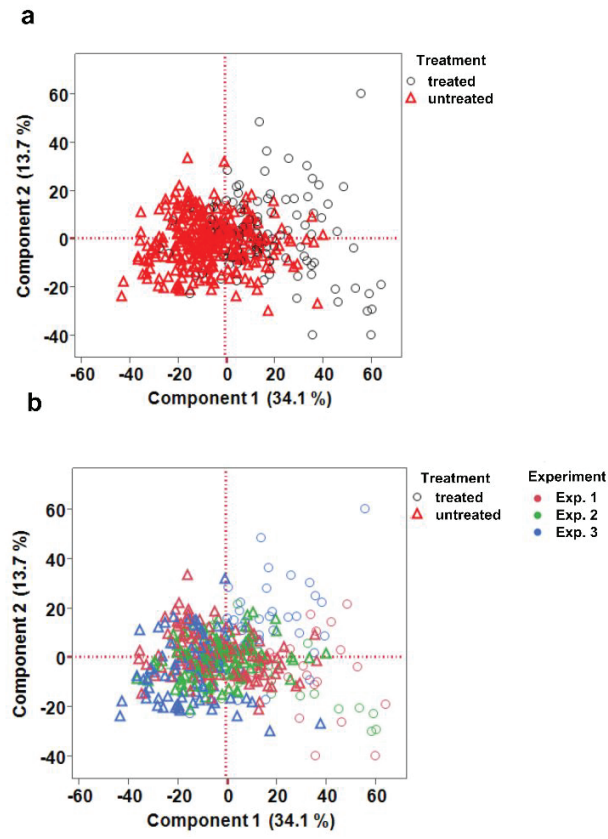
Figure S-3. Principal Component Analysis (PCA) of all single cells measured across three experiments. (**a**) Data points, all representing the average spectrum of a single cell, were shaped and colored depending on the culture conditions (in presence or absence of tamoxifen). Circle dots are cells cultured in the presence of tamoxifen, and triangles are cells cultured without. (**b**) Data points are colored differently depending on the experiment replicate. Circle dots are cells cultured in the presence of tamoxifen, and triangles are control cells.
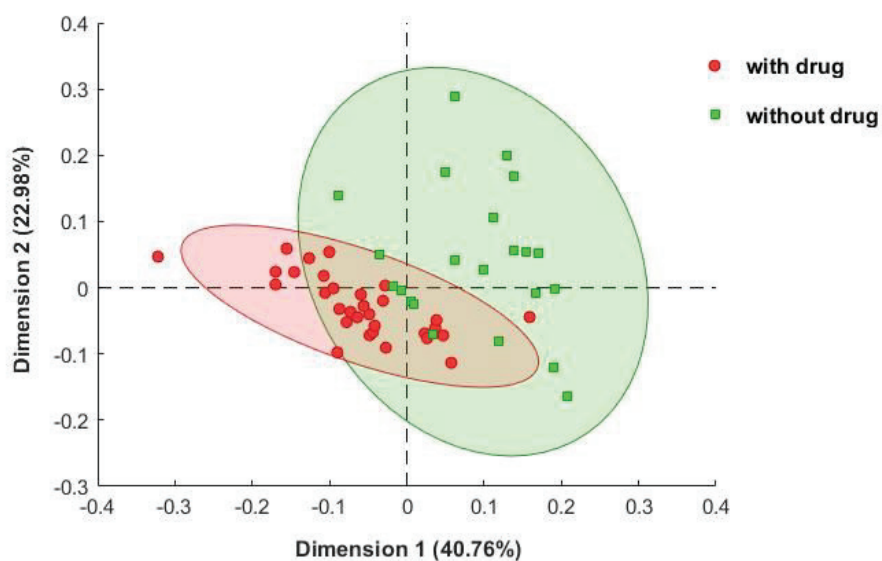
Figure S-4. PLS-DA analysis of 53 cells isolated by MS after Raman measurements**.** Each point represents the spectral data of single cells plotted onto two dimensions. Ellipses shows that cells under drug influence and control cells formed two distinct clusters. Square dots represent cells used as a control (no drug treatment), while square show cells that underwent tamoxifen treatment. Ellipses represent 95% confidence interval for each cluster.
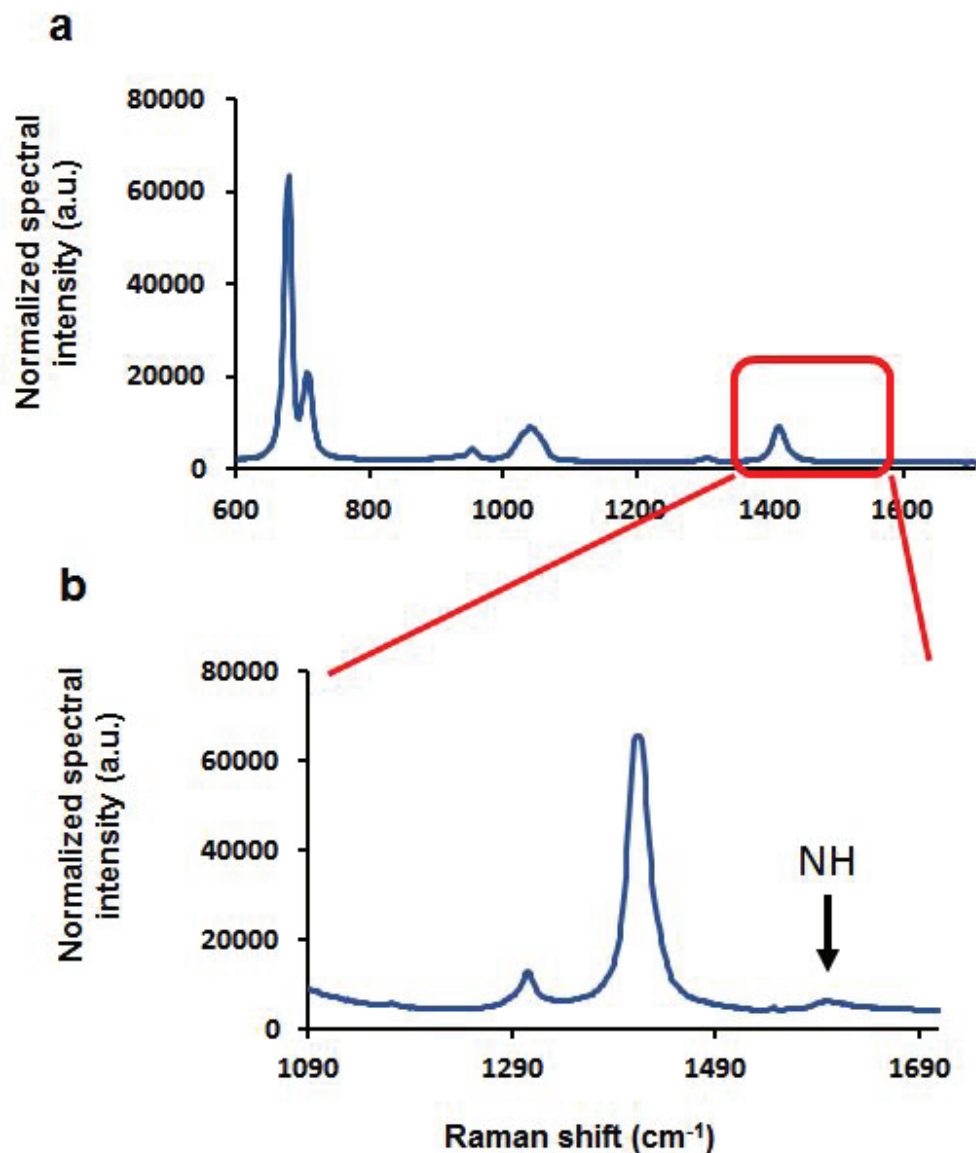
Figure S-5. Raman spectrum of purified tamoxifen drug (10% concentration). a) spectral profile of tamoxifen obtained with a 532 nm laser over the range of the fingerprint region. It shows a strong dominant peak at 677 cm^{-1} that we could not identify. b) Over a narrow range the CC chain associated peak at 1601 cm^{-1} could be seen although very weak in by comparison to other peaks. A strong peak at 1418 cm^{-1} was found.
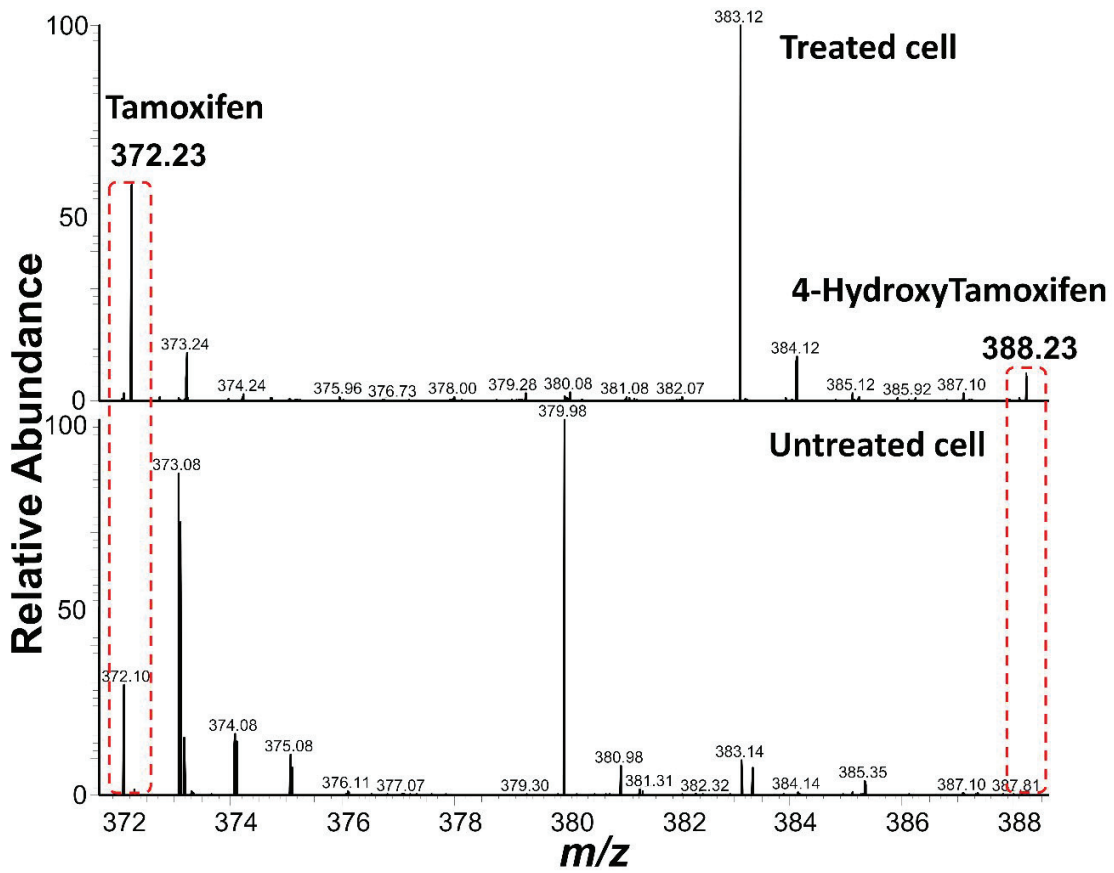
Figure S-6. Tamoxifen and 4-OHT peaks in full scan mode in tamoxifen-treated cell. An untreated cell spectrum is shown as control.
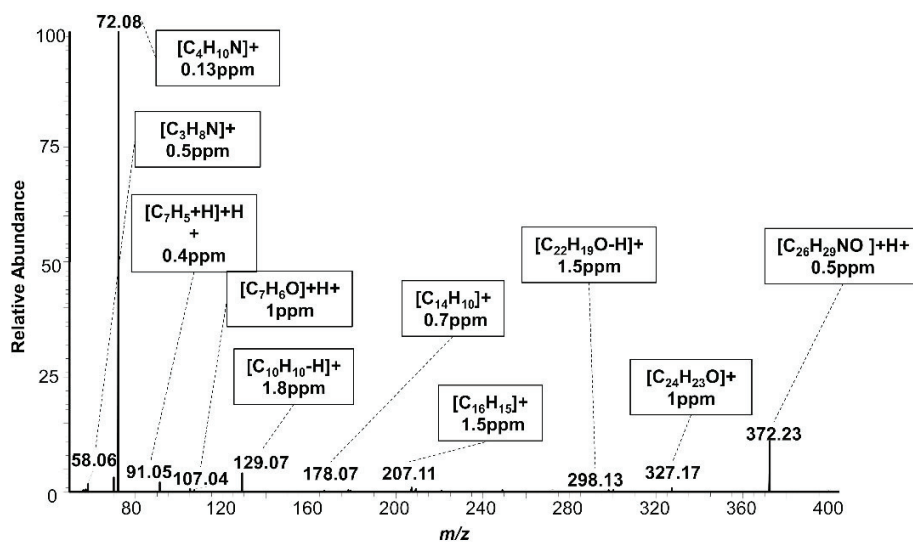
Figure S-7. Tamoxifen fragmentation profile. Tamoxifen's presence in single cell was verified by its 9 unique fragments.
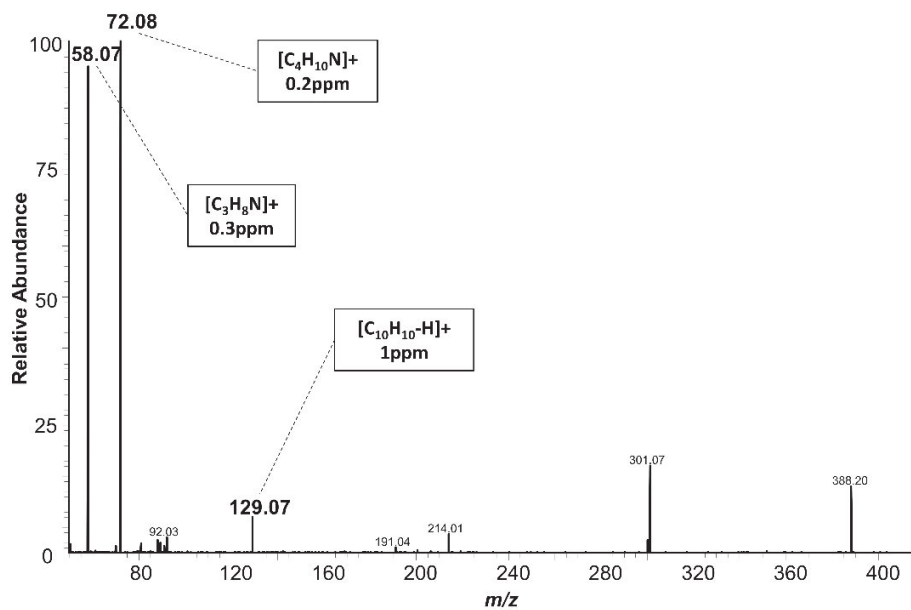
Figure S-8. 4-OHT fragmentation profile indicated three unique fragments that were used for positive identification.
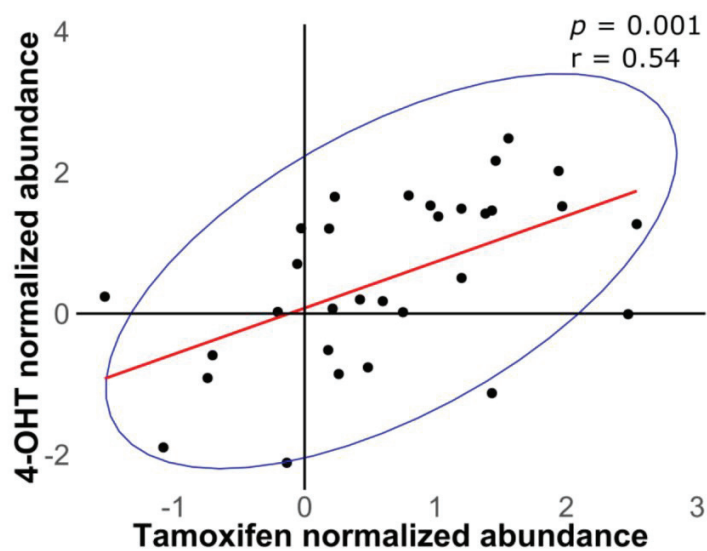
Figure S-9. Relation between tamoxifen and 4-OHT concentrations in single cells treated with tamoxifen. A significant positive correlation (r = 0.54, p = 0.0007) could be observed between tamoxifen and its metabolite. The red line represents the linear regression. The ellipse represents 95% confidence.
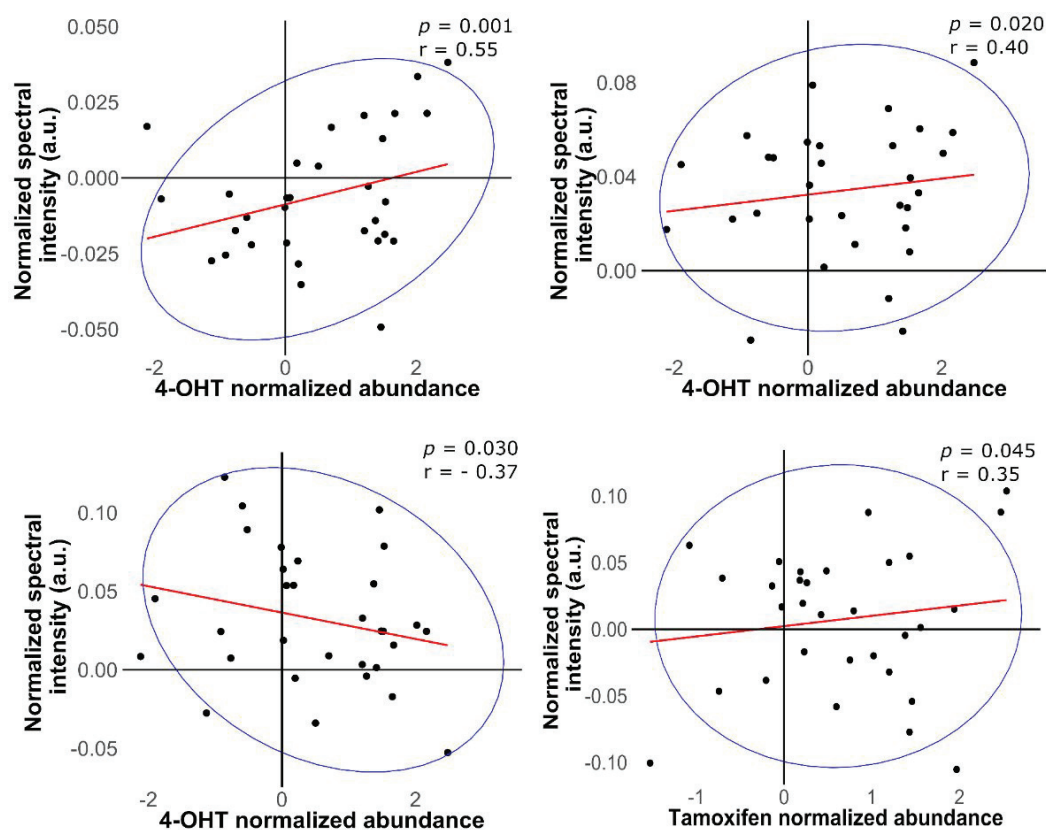
Figure S-10. Correlation plots between Raman spectral differences and abundances of tamoxifen or 4-OHT. Raman spectral differences between the two conditions (with and without tamoxifen) were used for correlations. Four major peaks with significant correlations ($p = 0.05$) were chosen. a) 4-OHT abundance correlates positively with the peak at 1001 cm^{-1} associated to aromatic compounds and proteins. b) 4-OHT correlates with peak at 1236 cm^{-1} associated to the nucleic acid, protein and lipids c) 4-OHT negatively correlates with 1545 cm^{-1} associated to proteins. d) Tamoxifen abundance in single-cells positively correlates with the peak at 1651 cm^{-1} associated to the Amide I of proteins. Ellipses represent 95% confidence. Redlines represent linear regression.
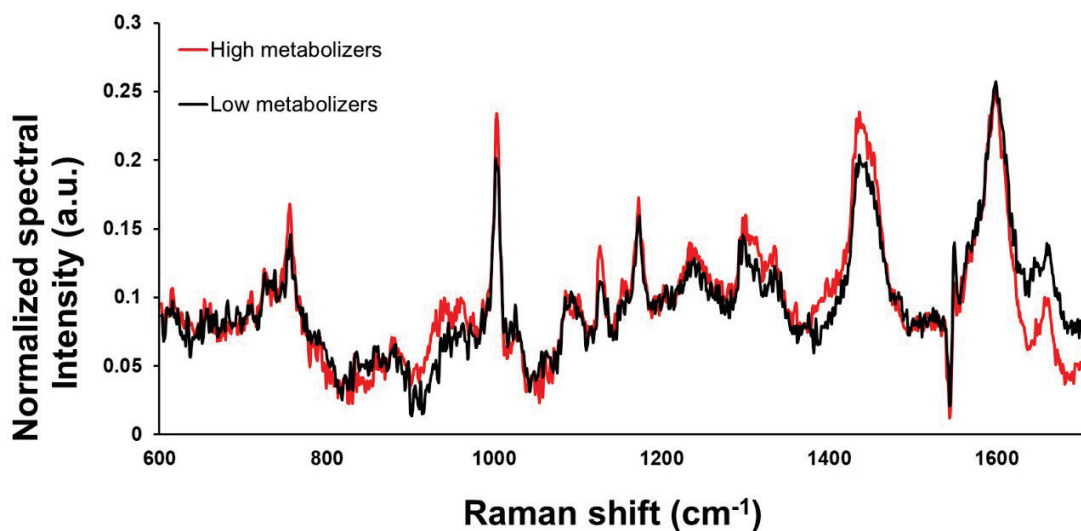
Figure S-11. Average, background-subtracted Raman spectrum of high (n = 8) and low (n = 8) metabolizers of tamoxifen. The high and low metabolizers were identified the ratio of metabolized to unmetabolized tamoxifen in each cell. Significant differences could be found (ANOVA, Tukey HSD $p < 0.05$) for several peaks, such as for the aromatic compounds peak at 1001 cm^{-1}, the lipid/protein peak at 1445 cm^{-1}, and the cytochrome peak at 752 cm^{-1} which were also identified in Figure 2 and 3.